

Harmonic-Constrained Three-Level Optimized Pulse Patterns for Grid-Connected Converters with *LCL* Filters

Shirin Rahmanpour, *Student Member, IEEE*, Petros Karamanakos, *Senior Member, IEEE*,
and Tobias Geyer, *Fellow, IEEE*

Abstract—This paper presents the computation of three-level optimized pulse patterns (OPPs) for converters connected to the grid via *LCL* filters. To this aim, the conventional OPP optimization problem is reformulated to account for the transfer function from the switching signal harmonics to the grid current harmonics. In addition, by incorporating constraints on grid current harmonics into the proposed OPP optimization problem, compliance with harmonic grid standards is ensured. Moreover, the restrictions that are typically imposed on multilevel switching signals, i.e., quarter-wave symmetry and unipolar switch positions, are relaxed in the proposed problem. This relaxation enables a reduction in current harmonic distortions within certain modulation intervals compared to conventional OPPs that do not limit grid current harmonics. The presented numerical results and real-time tests demonstrate the superior harmonic performance of the proposed harmonic-constrained relaxed OPPs, outperforming not only conventional modulation methods, such as space vector modulation (SVM), but also selective harmonic elimination (SHE) and conventional OPPs. Finally, further investigations reveal that the proposed OPPs maintain compliance with harmonic grid standards, even under variations in system parameters or when the *LCL* filter is downsized.

Index Terms—Grid-connected converters, grid standards, harmonic distortions, *LCL* filter, medium-voltage converters, optimized pulse patterns (OPPs), pulse width modulation (PWM).

I. INTRODUCTION

MEDIUM-VOLTAGE (MV) converters, with power ratings exceeding 1 MVA, are typically operated at very low switching frequencies (well below 1 kHz) to keep the switching losses low. However, the harmonic performance of conventional modulation techniques, such as carrier-based pulse width modulation (CB-PWM) or space vector modulation (SVM), significantly deteriorates at low pulse numbers, i.e., at low ratios of switching-to-fundamental frequency [1]. To improve the trade-off between switching frequency and the harmonic distortions of converter outputs, programmed PWM methods, such as selective harmonic elimination/mitigation (SHE/SHM) [2]–[5] and optimized pulse patterns (OPPs) [6]–[9], can be employed. These advanced modulation techniques

determine the switching angles, i.e., switching time instants, of the switching signal through offline mathematical procedures, enabling better harmonic performance compared to conventional methods.

Specifically, SHE/SHM methods compute the switching angles by solving a system of nonlinear equations/inequalities aimed at eliminating/mitigating specific harmonics. In contrast, the switching angles of OPPs are computed through an optimization problem aimed at minimizing the output current total demand distortion (TDD). Since OPPs are obtained by minimizing the entire harmonic content of the output current, they demonstrate superior harmonic performance compared to other modulation schemes [10], [11].

Nevertheless, when grid-connected converters are of interest, both SHE/SHM-based pulse patterns and OPPs face the challenge of ensuring that the output current complies with harmonic grid standards, such as the IEEE 519 standard [12]. These standards set limits on current and/or voltage harmonics as well as on TDDs at the point of common coupling (PCC), with the goal of reducing the harmonics injected into the grid. Hence, compliance is crucial in preventing grid customers from adversely affecting each other, underscoring the importance of adhering to such standards.

To address this challenge—at least partly—SHM methods have been proposed to produce a current that complies with harmonic grid standards [13]–[15]. More specifically, the methods in [13] and [14] attempt to fulfill grid standards by adjusting the dc-link voltage, i.e., the modulation index. In doing so, however, the operational range of the converter is limited. In contrast, [15] achieves compliance over the whole range of modulation indices by employing a cascaded H-bridge converter with variable dc-links. Moreover, [16] and [17] aim not only to meet grid standards but also to account for the grid non-idealities (i.e., grid voltage harmonics) while shaping desired harmonic spectra. These techniques help improve the quality of the converter output current. Nevertheless, fully meeting harmonic grid standards requires a high number of pulses, posing a challenge for most SHE/SHM methods as solving the associated system of equations/inequalities is complex, if not infeasible. Alternatively, the modulation schemes in [18] and [19] mitigate this issue by computing the switching angles such that the difference between selected harmonic amplitudes and the maximum levels allowed by grid standards is minimized.

Nevertheless, in all the aforementioned techniques, the

The work of Shirin Rahmanpour and Petros Karamanakos was supported by the Research Council of Finland.

Shirin Rahmanpour and Petros Karamanakos are with the Faculty of Information Technology and Communication Sciences, Tampere University, 33101 Tampere, Finland; e-mail: shirin.rahmanpour@tuni.fi, p.karamanakos@ieee.org.

Tobias Geyer is with ABB System Drives, 5300 Turgi, Switzerland; e-mail: t.geyer@ieee.org.

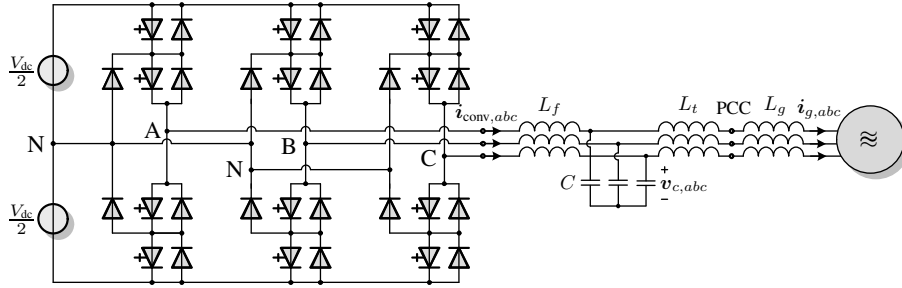


Fig. 1: Three-level voltage-source NPC converter connected to the grid via an LC filter and a transformer.

switching signals are obtained for first-order systems, i.e., by assuming an inductive load. As a result, their harmonic performance can be compromised when higher-order systems, such as grid-connected converters equipped with LCL filters,¹ are considered. Although these filters effectively attenuate high-order harmonics, they still do not guarantee compliance with harmonic grid standards as low-order harmonics may exceed their specified limits.

Considering the above, only a few works have incorporated harmonic LCL filters into the OPP computation process, see [20] and [21]. In [20], OPPs are tailored for higher-order systems by including the LCL filter transfer function from the switching signal to the grid current in the objective function of the optimization problem. In doing so, the quality of the output current is significantly improved. However, it is not ensured that the computed OPPs produce grid currents that abide by specific harmonic standards. To tackle this issue, the OPP optimization problem in [21] is enhanced by explicitly adding constraints on the grid current harmonics, while still accounting for the LCL filter. This guarantees that the grid current harmonics remain within the limits dictated by the harmonic grid standards. Moreover, the artificial restrictions that are typically imposed on multilevel OPPs, such as quarter-wave symmetry (QWS) and unipolar switch positions, are relaxed in that work. As a result, the expected increase in current TDD due to the additional harmonic limitations is mitigated.

This paper builds on [21] by providing a deeper discussion on the OPP problem formulation and a more comprehensive performance assessment to better highlight its benefits. The key contributions are:

- The computation of OPPs with relaxed properties for grid-connected three-level converters with LCL filters, ensuring (a) high-quality grid currents, and (b) compliance with harmonic grid standards by explicitly constraining individual current harmonics.
- Introduction of soft constraints on current harmonics to mitigate numerical and feasibility problems in the OPP optimization process.
- A detailed assessment of the performance of the computed OPPs in a real-time hardware-in-the-loop (HIL) environment.
- Robustness analysis under different conditions, such as variations in the grid impedance and filter components as

¹In practice, for MV applications, the converter is connected to the grid via an LC filter and a transformer, resulting in an LCL configuration.

well as a smaller harmonic filter.

- Benchmarking of the proposed modulation method against SVM as well as SHE and conventional OPPs without harmonic constraints.

As the results demonstrate, the proposed harmonic-constrained relaxed OPPs ensure compliance with harmonic grid standards across all tested conditions. This is in stark contrast to the benchmarked modulation methods, which tend to violate individual harmonic limits. Moreover, on top of this favorable feature, the proposed OPPs can even achieve lower current TDD than conventional OPPs without harmonic constraints for certain modulation intervals.

This article is structured as follows. Section II models a grid-connected converter equipped with an LCL filter, which serves as the basis for formulating the OPP optimization problems. In the same section, the optimization problem for the conventional OPPs that account for the harmonic filter is presented, followed by the proposed formulation for harmonic-constrained OPPs with relaxed properties. Sections III and IV present and discuss the numerical results and real-time tests, respectively, while comparing the performance of the proposed OPPs with that of other PWM schemes. A critical discussion on the limitations of the proposed modulation technique, along with potential future research directions, is provided in Section V. Finally, Section VI concludes the paper.

II. OPPS FOR GRID-CONNECTED CONVERTERS WITH LCL FILTERS

The OPPs discussed in this paper are computed for an MV power electronic system that comprises a three-level voltage-source neutral-point-clamped (NPC) converter connected to the grid via an LCL filter, as illustrated in Fig. 1. In the sequel of this section, the model of the system under consideration is derived, which will be subsequently used for formulating the optimization problems for both the conventional and proposed OPPs.

A. Modeling of the Grid-Connected Converter System

The $\alpha\beta$ -frame equivalent circuit of the considered system is shown in Fig. 2.² Therein, Fig. 2(a) is the equivalent circuit for both fundamental and harmonic components, whereas Fig. 2(b) represents only the harmonic model. The latter serves

²For the sake of notational simplicity, the $\alpha\beta$ subscript is omitted for variables in the $\alpha\beta$ -frame, whereas variables in the abc -frame retain their respective subscript.

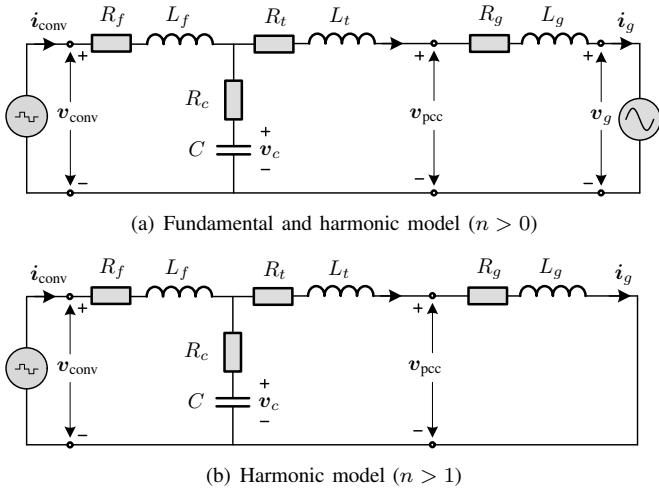


Fig. 2: Equivalent circuit of the converter system in the $\alpha\beta$ -frame.

as the basis for the subsequent. Note that, since the grid voltage v_g is assumed to be ideal, i.e., it is ripple-free, it appears as a short-circuit in the harmonic model.

Regarding the equivalent circuit in Fig. 2(b), the differential equations that describe the dynamics of the system are

$$L_f \frac{di_{\text{conv}}(t)}{dt} = -R_1 i_{\text{conv}}(t) + R_c i_g(t) - v_c(t) + v_{\text{conv}}(t) \quad (1a)$$

$$L_{gt} \frac{di_g(t)}{dt} = R_c i_{\text{conv}}(t) - R_2 i_g(t) + v_c(t) \quad (1b)$$

$$\frac{dv_c(t)}{dt} = \frac{1}{C} i_{\text{conv}}(t) - \frac{1}{C} i_g(t), \quad (1c)$$

where i_{conv} is the converter current, i_g the grid current, and v_c the capacitor voltage. Moreover, v_{conv} is the converter output voltage given by

$$v_{\text{conv}}(t) = \frac{V_{\text{dc}}}{2} \mathbf{K} \mathbf{u}_{abc}(t), \quad (2)$$

with V_{dc} being the dc-link voltage of the converter, and $\mathbf{u}_{abc} = [u_a \ u_b \ u_c]^T \in \{-1, 0, 1\}^3$ the three-phase switching signal. In addition, \mathbf{K} is the reduced Clarke transformation matrix

$$\mathbf{K} = \frac{2}{3} \begin{bmatrix} 1 & -\frac{1}{2} & -\frac{1}{2} \\ 0 & \frac{\sqrt{3}}{2} & -\frac{\sqrt{3}}{2} \end{bmatrix}$$

that maps quantities in the three-phase (abc) frame, i.e., $\boldsymbol{\xi}_{abc} = [\xi_a \ \xi_b \ \xi_c]^T$, to quantities $\boldsymbol{\xi}_{\alpha\beta} = [\xi_\alpha \ \xi_\beta]^T$ in the stationary orthogonal ($\alpha\beta$) frame. Moreover, $R_1 = R_f + R_c$ in (1) includes the resistances R_f and R_c of the filter inductance L_f and capacitance C , respectively, while $R_2 = R_c + R_g + R_t$ is the combination of R_c with the grid R_g and transformer R_t resistances. Furthermore, the lumped inductance $L_{gt} = L_g + L_t$ combines the inductances of the grid L_g and transformer L_t , respectively.

Based on the above, the dynamics of the system in Fig. 2(b) can be characterized using the state vector $\mathbf{x} = [i_{\text{conv}}^T \ i_g^T \ v_c^T]^T \in \mathbb{R}^6$, while the grid current is chosen as the system output, i.e., $\mathbf{y} = i_g \in \mathbb{R}^2$. Considering the three-phase

switching signal \mathbf{u}_{abc} as the input, the state-space model of the system in question is given as

$$\begin{aligned} \frac{d\mathbf{x}(t)}{dt} &= \mathbf{A} \mathbf{x}(t) + \mathbf{B} \mathbf{u}_{abc}(t) \\ \mathbf{y}(t) &= \mathbf{C} \mathbf{x}(t), \end{aligned} \quad (3)$$

where the state-space matrices \mathbf{A} , \mathbf{B} , and \mathbf{C} are obtained from (1). With (3), the transfer matrix from the system input, i.e., the three-phase switching signal \mathbf{u}_{abc} , to its output, i.e., the grid current i_g , can be derived as

$$\mathbf{H}(s) = \mathcal{L}\{i_g\}(s) / \mathcal{L}\{\mathbf{u}_{abc}\}(s), \quad (4)$$

which facilitates mapping the effect of the applied (to-be-computed) pulse pattern on the grid current harmonics.

With (4), the grid current in the frequency domain can be expressed as

$$i_g(s) = \mathbf{H}(s) \mathbf{u}_{abc}(s),$$

which, when transformed to the abc -frame, becomes

$$i_{g,abc}(s) = \mathbf{K}^{-1} i_g(s) = \mathbf{G}(s) \mathbf{u}_{abc}(s), \quad (5)$$

with \mathbf{K}^{-1} being the inverse reduced Clarke transformation matrix. It is noteworthy that, by substituting s with $j n \omega_g$ in $\mathbf{G}(s)$ —where ω_g is the grid angular frequency—the impact of the n^{th} switching signal (i.e., pulse pattern) harmonic on the n^{th} grid current harmonic can be analyzed.

B. Three-Level OPPs that Consider the LCL Filter

Consider a three-phase symmetric, 2π -periodic switching signal $\mathbf{u}_{abc} = [u_a \ u_b \ u_c]^T$. Due to this symmetry, it suffices to compute the single-phase switching signal $u(\theta) \equiv u_a(\theta)$, since the switching signals for phases b and c can be obtained by phase-shifting $u_a(\theta)$ by $-2\pi/3$ and $2\pi/3$, respectively.

Conventional OPPs are computed such that the single-phase switching signal $u(\theta)$ exhibits quarter- and half-wave symmetry (QaHWS). In addition, for multilevel converters, it is common practice to consider only non-negative switch positions in the positive half-wave of the fundamental period and vice versa in the negative half-wave. This gives rise to unipolar pulse patterns.

With these constraints, the three-level switching signal can be fully described by d switching angles $\alpha_i \in [0, \pi/2]$, $i \in \{1, \dots, d\}$, and $d + 1$ switch positions $u_i \in \{0, 1\}$, $i \in \{0, \dots, d\}$, while the initial switch position is assumed to be zero, i.e., $u_0 = 0$. Here, d denotes the number of switching transitions $\Delta u_i = u_i - u_{i-1} \in \{-1, 1\}$, occurring at each switching angle, in the first quarter of the fundamental period. Thus, for QaHWS pulse patterns with unipolar switch positions, it follows that $\Delta u_i = (-1)^{i+1}$, $i \in \{1, \dots, d\}$.

Given the above, the single-phase three-level QaHWS unipolar switching signal $u(\theta)$ can be expressed using the following Fourier series expansion

$$u(\theta) = a_0 + \sum_{n=1}^{\infty} (a_n \cos(n\theta) + b_n \sin(n\theta)). \quad (6)$$

It can be shown that, due to the QaHWS, the a_n Fourier coefficients in (6) are equal to zero, while the b_n coefficients

are nonzero only for odd harmonics. These coefficients are given by³

$$b_n = \frac{4}{n\pi} \sum_{i=1}^d (-1)^{i+1} \cos(n\alpha_i), \quad n = 1, 3, 5, \dots \quad (7)$$

Hence, the amplitude of the n^{th} harmonic of the single-phase switching signal $u(\theta)$ is $\hat{u}_n = |b_n|$, resulting in the n^{th} converter voltage harmonic with the amplitude of $\hat{v}_n = (V_{\text{dc}}/2) \hat{u}_n$. Consequently, the amplitude of the n^{th} a -phase grid current harmonic can be determined using (5) and (6), according to

$$\hat{i}_{g,a,n} = g_n \hat{u}_n, \quad (8)$$

where g_n is the norm of the transfer matrix $\mathbf{G}(jn\omega_g)$ for each harmonic order n .

OPPs are commonly computed such that they produce an output current with the lowest possible TDD, defined as

$$I_{\text{TDD}} = \frac{1}{\sqrt{2}I_{\text{nom}}} \sqrt{\sum_{n \neq 1} \hat{i}_{a,n}^2}, \quad (9)$$

with I_{nom} being the rms value of the nominal current, and $\hat{i}_{a,n}$ the amplitude of the n^{th} a -phase output current harmonic, i.e., the grid current $\hat{i}_{g,a,n}$ in this work. Since $\hat{i}_{g,a,n}$ is related to the amplitude of the n^{th} switching signal harmonic \hat{u}_n through the gain g_n (see (8)), the grid current TDD is

$$I_{\text{TDD}} = \underbrace{\frac{2\sqrt{2}}{\pi I_{\text{nom}}}}_c \sqrt{\sum_{n=5,7,\dots} \left(\frac{g_n}{n} \sum_{i=1}^d (-1)^{i+1} \cos(n\alpha_i) \right)^2}. \quad (10)$$

Note that, in (10), the triplen current harmonics—those harmonics of order that are integer multiples of three—are not considered. This is due to the fact that they do not drive harmonic currents in a three-phase balanced system, where it is assumed that the load is in a wye configuration with a floating star point.

The current TDD in (10) can be expressed as $I_{\text{TDD}} = c \sqrt{J_{\text{QaHWS}}}$, where c depends only on the nominal current. The constant c can be discarded in the optimization process since it does not affect the outcome. Consequently, J_{QaHWS} becomes the objective function of the OPP optimization problem. By doing so, the QaHWS unipolar OPPs that produce the minimum grid current TDD while accounting for the LCL filter are computed by solving the following non-convex optimization problem

$$\underset{\alpha_Q = [\alpha_1 \dots \alpha_d]^T}{\text{minimize}} \quad J_{\text{QaHWS}} \quad (11a)$$

$$\text{subject to} \quad b_1 = \frac{4}{\pi} \sum_{i=1}^d (-1)^{i+1} \cos(\alpha_i) = m \quad (11b)$$

$$0 \leq \alpha_1 \leq \alpha_2 \leq \dots \leq \alpha_d \leq \frac{\pi}{2}, \quad (11c)$$

where (11b) ensures that the desired modulation index $m \in [0, 4/\pi]$ is synthesized, while the $d + 1$ inequality constraints (11c) guarantee that the switching angles are in ascending order. In addition, owing to the imposed QaHWS and unipolar switch positions, only the switching angles α_Q in the first quarter of the fundamental period are treated as the optimization variables. Notably, the inclusion of the gain g_n in the objective function of problem (11) enables the computation of OPPs for higher-order systems, such as the system considered in this paper (see Fig. 1).

C. Relaxed OPPs that Meet Harmonic Grid Standards

As shown in [22], relaxing QWS and dropping the switching restrictions that are typically imposed on multilevel switching signals increases the degrees of freedom in the three-level OPP optimization problem. Consequently, the current TDD can be further reduced. Nevertheless, by discarding QWS, and thus considering only half-wave symmetry (HWS) for the switching signal, $2d$ switching angles $\alpha_i \in [0, \pi], i \in \{1, \dots, 2d\}$, need to be computed in the first half of the fundamental period, as opposed to the d switching angles computed for QaHWS OPPs. In addition, permitting negative switch positions in the positive half-wave of the fundamental period and allowing $u_0 \in \{-1, 0, 1\}$ —thereby facilitating multipolar switch positions—results in $2^{d+1} - 2$ feasible switching sequences. Consequently, the HWS multipolar OPP optimization problem will not only have $2d$ switching angles, represented by $\alpha_H = [\alpha_1 \dots \alpha_{2d}]^T$, as optimization variables, but it also has to compute the optimal sequence $\mathbf{u}_H = [u_0 \dots u_{2d-1}]^T$ of $2d$ switch positions $u_i \in \{-1, 0, 1\}, i \in \{0, \dots, 2d-1\}$. Lastly, it is important to note that HWS necessitates that $u_{2d} = -u_0$.

With HWS, the Fourier coefficients of $u(\theta)$ in (6) remain zero for even harmonics, whereas for odd harmonics, they are given by

$$a_n = -\frac{2}{n\pi} \sum_{i=1}^{2d} \Delta u_i \sin(n\alpha_i), \quad n = 1, 3, 5, \dots \quad (12)$$

$$b_n = \frac{2}{n\pi} \sum_{i=1}^{2d} \Delta u_i \cos(n\alpha_i), \quad n = 1, 3, 5, \dots$$

Therefore, the amplitude of the n^{th} switching signal harmonic becomes $\hat{u}_n = \sqrt{a_n^2 + b_n^2}$. As a result, the current TDD for HWS multipolar OPPs is

$$I_{\text{TDD}} = \frac{\sqrt{2}}{\pi I_{\text{nom}}} \left(\underbrace{\sum_{n=5,7,\dots} \left(\frac{g_n}{n} \right)^2}_{c'} \left(\left(\sum_{i=1}^{2d} \Delta u_i \sin(n\alpha_i) \right)^2 + \left(\sum_{i=1}^{2d} \Delta u_i \cos(n\alpha_i) \right)^2 \right)^{1/2}, \quad (13)$$

which is of the form $I_{\text{TDD}} = c' \sqrt{J_{\text{HWS}}}$.

Even though the HWS multipolar OPPs, computed by minimizing J_{HWS} (see (13)), produce the minimum grid current TDD, they do not guarantee that individual current harmonics comply with harmonic grid standards. To ensure that grid current harmonics remain within the limits dictated by the IEEE

³For more details on the derivation of Fourier coefficients when imposing different symmetry properties, the reader is referred to [22].

519 standard, explicit constraints need to be integrated into the OPP optimization problem.⁴ In doing so, the harmonic-constrained three-level OPP optimization problem with HWS and multipolar switch positions is formulated as follows

$$\underset{\alpha_H, \mathbf{u}_H, \epsilon}{\text{minimize}} \quad J_{\text{HWS}} + \epsilon^T \mathbf{W} \epsilon \quad (14a)$$

$$\text{subject to} \quad b_1 = \frac{2}{\pi} \sum_{i=1}^{2d} \Delta u_i \cos(\alpha_i) = m \quad (14b)$$

$$a_1 = -\frac{2}{\pi} \sum_{i=1}^{2d} \Delta u_i \sin(\alpha_i) = 0 \quad (14c)$$

$$0 \leq \alpha_1 \leq \alpha_2 \leq \dots \leq \alpha_{2d} \leq \pi \quad (14d)$$

$$\hat{i}_{g,a,n} \leq \hat{i}_{n,\max} + \epsilon_n, \quad n = 6k \pm 1, k \in \mathbb{N}^+ \quad (14e)$$

$$\epsilon_n \geq 0 \quad (14f)$$

$$u_i \in \{-1, 0, 1\} \quad \forall i \in \{0, \dots, 2d-1\} \quad (14g)$$

$$\Delta u_i \in \{-1, 1\} \quad \forall i \in \{1, \dots, 2d\}, \quad (14h)$$

which aims to compute OPPs that produce grid currents with the lowest possible TDD while ensuring current harmonics respect grid standards as closely as possible. As can be observed, the optimization problem (14) is not only a non-convex problem—similar to problem (11)—but it is also mixed-integer due to the sequence of integer switch positions, i.e., $\mathbf{u}_H = [u_0 \dots u_{2d-1}]^T$, being part of the optimization variables. Nevertheless, to avoid solving a mixed-integer problem, a non-convex optimization problem is solved for each candidate sequence. The optimal pair of switching angles α_H^* and sequence of switch positions \mathbf{u}_H^* is the one that yields the lowest I_{TDD} . The procedure for computing the proposed three-level harmonic-constrained relaxed OPPs is described in Algorithm 1.

For the proposed OPPs to achieve the desired performance, constraints (14b) and (14c) are imposed to ensure that the fundamental OPP component has an amplitude equal to the desired modulation index m , while its initial phase is zero. Regarding the harmonic constraints (14e), the amplitudes of low-order non-triplen odd current harmonics in \mathbb{N}^+ are limited to the maximum levels allowed by grid standards, i.e., $\hat{i}_{n,\max}$. The harmonics at higher frequencies are effectively attenuated by the *LCL* filter and are thus not constrained in the optimization problem. Note that the limits $\hat{i}_{n,\max}$ can be adjusted to equip the computed OPPs with robustness against parameter variations that may impact their performance. For this purpose, the limits can be made tighter, e.g., considering a limit of $0.8 \hat{i}_{n,\max}$ instead of $\hat{i}_{n,\max}$.

Finally, it should be pointed out that soft constraints are imposed on individual current harmonics in the OPP optimization problem (14). This is in contrast to [21] where hard constraints are utilized instead. This approach is adopted in this work to prevent feasibility issues that may arise during the optimization process when hard constraints are present. To minimize constraint violations, the slack variables ϵ_n

⁴Note that the proposed harmonic-constrained OPP optimization problem can be adapted to comply with any grid standards, as only the harmonic limits need to be adjusted accordingly.

Algorithm 1 Computation of three-level harmonic-constrained relaxed OPPs

- 1: Given equidistant-gridded modulation interval $m \in [0, \frac{4}{\pi}]$
e.g., $m = 0 : \frac{1}{64\pi} : \frac{4}{\pi}$
 - 2: **for** each m **do**
 - 3: **for** each candidate sequence of switch positions
 \mathbf{u}_H **do**
 - 4: Solve the OPP optimization problem (14) multiple times using the Matlab function `fmincon`, each time with a randomly initialized set of angles.
 - 5: **end for**
 - 6: **return** the optimal sequence of switch positions \mathbf{u}_H^* and corresponding optimal switching angles α_H^* result in the minimum I_{TDD}
 - 7: **end for**
-

TABLE I: Rated values of the system

Parameter	Symbol	SI Value
Voltage	V_R	3.15 kV
Current	I_R	1.65 kA
Angular grid frequency	ω_{gR}	$2\pi 50$ rad/s
Short-circuit ratio	k_{sc}	15
Grid impedance ratio	k_{XR}	10

TABLE II: System parameters

Grid	Inductance	L_g	349.19 μH
	Resistance	R_g	10.97 $\text{m}\Omega$
<i>LC</i> filter	Inductance	L_f	350 μH
	Inductor resistance	R_f	0.3 $\text{m}\Omega$
	Capacitance	C	420 μF
	Capacitor resistance	R_c	4 $\text{m}\Omega$
Transformer	Inductance	L_t	526.41 μH
	Resistance	R_t	16.54 $\text{m}\Omega$

for $n = 6k \pm 1, k \in \mathbb{N}^+$ —aggregated into the vector ϵ —are introduced alongside the diagonal weighting matrix \mathbf{W} . The latter is designed to heavily penalize violations of soft constraints, aiming to ensure that the constrained individual current harmonics remain below their permissible levels as much as possible. As a result, the slack variables ϵ are also treated as optimization variables.

III. VALIDATION THROUGH NUMERICAL RESULTS

In this section, the performance of different PWM schemes is assessed through numerical simulations. More specifically, the benchmarked methods include the conventional (QaHWS unipolar) OPPs computed using (11), the proposed harmonic-constrained relaxed OPPs obtained by solving (14), SHE, and SVM. Note that SVM is implemented by means of asymmetric regularly sampled CB-PWM with appropriate common-mode voltage injection [1].

All the above-mentioned PWM methods are employed to modulate an MV three-level NPC converter connected to the grid via an *LCL* filter, see Fig. 1. The rated values and system parameters are provided in Tables I and II, respectively. The converter has a rated power of 9 MVA and a dc-link voltage of 4.84 kV. As for the *LCL* filter, its resonance frequency is

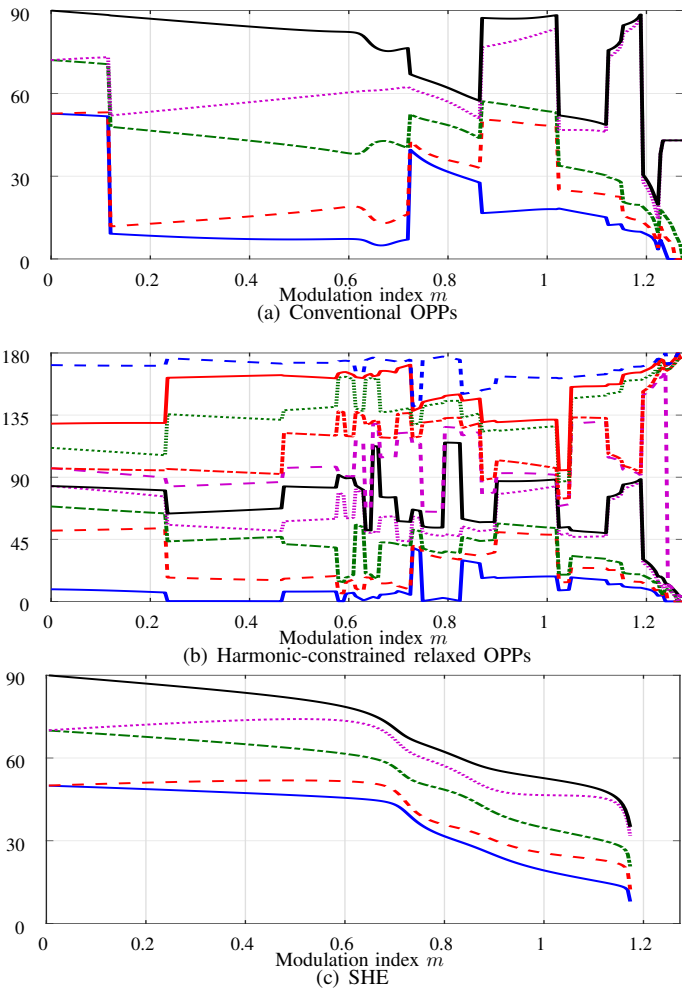


Fig. 3: Primary switching angles (in degrees) of (a) the conventional OPPs, (b) the proposed harmonic-constrained relaxed OPPs, and (c) SHE. The bottom lines (solid blue) in (a)–(c) represent the primary switching angle α_1 , while the second lines (dashed red) correspond to α_2 , and so forth. Note that the top lines (solid black) in (a) and (c) correspond to α_5 , whereas the top line (dashed blue) in (b) corresponds to α_{10} due to the need to compute twice the number of switching angles for the HWS.

$f_{\text{res}} = 535$ Hz, as can be deduced from the parameters listed in Table II.

For a meaningful analysis and fair comparison, all PWM methods are evaluated under the same switching frequency of $f_{\text{sw}} = 250$ Hz. With a fundamental frequency of $f_1 = 50$ Hz, this setting implies that $d = 5$ for the OPPs, while the SHE-based pulse patterns are computed such that the 5th, 7th, 11th, and 13th harmonics are eliminated. In addition, the OPP optimization problems (11) and (14) are solved for 500 initial points. Moreover, the infinite sum in the objective function is approximated by including the first 500 harmonics, as higher-order current harmonics are negligible. It is noteworthy that problem (14) constrains all non-zero grid current harmonics up to the 25th one. Furthermore, the weighting matrix is assumed to be $\mathbf{W} = 500\mathbf{I}_8$, with \mathbf{I}_8 denoting the identity matrix of dimension eight.

The optimal switching angles obtained by solving the OPP optimization problems (11) and (14) are depicted in Figs. 3(a) and 3(b), respectively, for modulation indices in the interval $[0, 4/\pi]$. In addition, the d switching angles obtained using

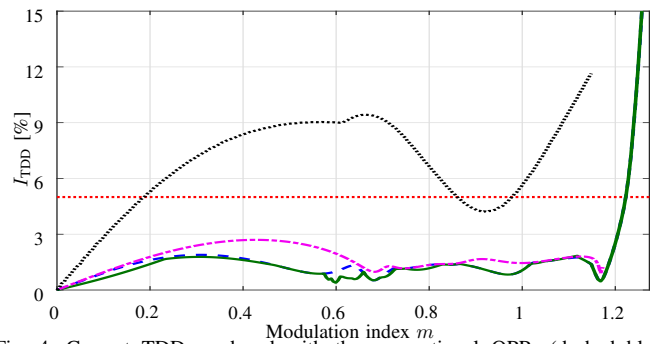


Fig. 4: Current TDD produced with the conventional OPPs (dashed blue line), harmonic-constrained relaxed OPPs (solid green line), SHE (dash-dotted magenta line), and SVM (dotted black line). The maximum current TDD allowed by the IEEE 519 standard is shown with the dotted red line.

the SHE method are shown in Fig. 3(c). As can be seen, the maximum modulation index achievable with SHE is limited to $m = 1.17$ out of $4/\pi$, indicating an underutilization of the dc-link voltage. In contrast, OPPs are applicable over the whole modulation range.

In addition, the grid current TDD I_{TDD} resulted from the aforementioned PWM methods is compared in Fig. 4 for $m \in [0, 4/\pi]$. As observed, the proposed harmonic-constrained relaxed OPPs produce a current TDD very close to that of the conventional OPPs without current harmonic constraints. More importantly, in some modulation intervals, the proposed OPPs outperform the conventional OPPs, while they outperform SHE and SVM methods over the whole modulation range. It is worth noting that the expected deterioration in current quality—due to constraining individual current harmonics—is effectively mitigated or even avoided. This is achieved through the additional degrees of freedom introduced in (14) by removing the traditionally imposed artificial restrictions on pulse patterns. As a result, the current TDD produced by the harmonic-constrained relaxed OPPs remains significantly below the 5% limit imposed by the IEEE 519 standard [12] as long as $m < 1.22$. Beyond that modulation index, the grid current TDD starts increasing considerably as six-step operation approaches. Nevertheless, since such high modulation indices are not typically used for grid-connected converters, it can be concluded that the proposed OPPs successfully meet the desired I_{TDD} limit.

Specifically, since grid-connected converters are typically operated to balance effective voltage utilization and harmonic distortions, the primary focus is on the modulation range $m \in [0.7, 1.15]$, with $m > 1$ being the most common. For this reason, Fig. 5 illustrates the single-phase pulse patterns obtained from the examined PWM schemes over one period for $m = 1.1185$. As shown in Fig. 5(b), the proposed OPPs (see problem (14)) exhibit HWS, unlike the other pulse patterns. Notably, even though the OPP problem (14) allows for various switching sequences, the unipolar sequence is optimal at this modulation index. In fact, when the converter operates exclusively at $m > 0.9$, the optimal sequence is the unipolar one, suggesting that multipolar OPPs are unnecessary. This observation enables the reduction of the computational complexity of proposed OPP problem. Nevertheless, when lower modulation indices are of interest, multipolar switching

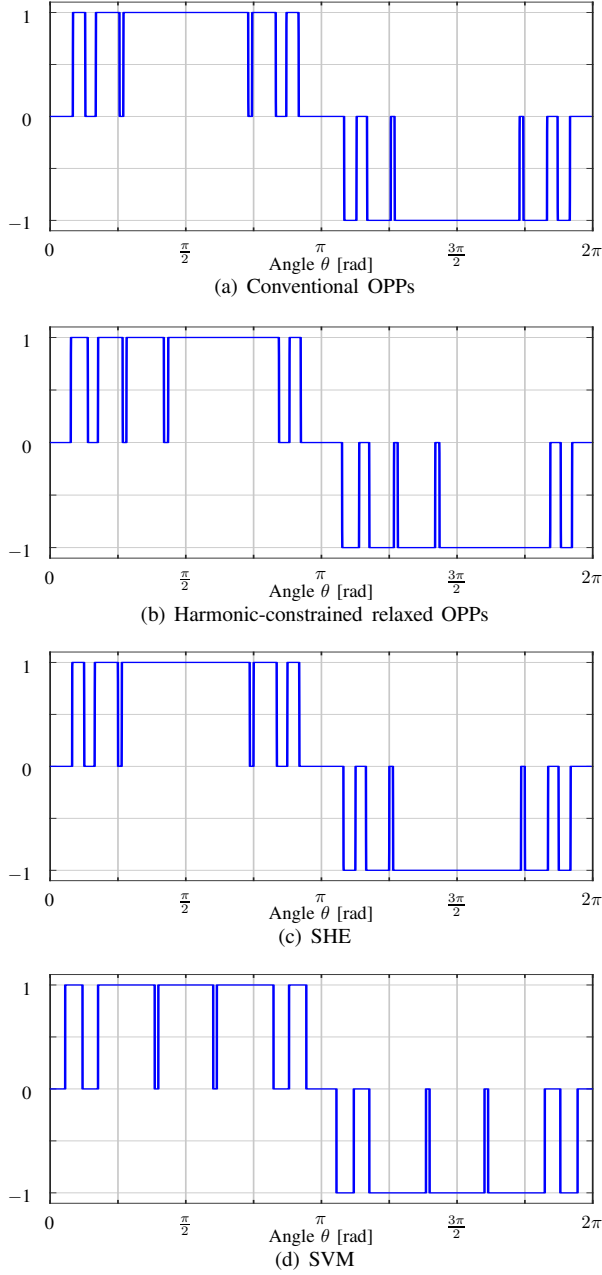


Fig. 5: Pulse patterns with $f_{sw} = 250$ Hz for $m = 1.1185$ obtained from (a) the conventional OPP optimization problem, (b) the harmonic-constrained relaxed OPP optimization problem, (c) SHE, and (d) SVM.

patterns become optimal over certain modulation ranges, i.e., $m \in [0, 0.47] \cup [0.58, 0.66] \cup [0.7, 0.73] \cup [0.75, 0.82]$. For example, Fig. 6 shows the pulse patterns for $m = 0.79$, where a negative switch position appears in the first half of the fundamental period, indicating that the optimal pattern is multipolar (see Fig. 6(b)).

IV. PERFORMANCE ASSESSMENT THROUGH REAL-TIME TESTS

In this section, the harmonic performance of the discussed PWM methods is assessed in a real-time HIL environment. This setup (illustrated in Fig. 7) uses a dSPACE SCALEXIO system equipped with a 2.8 GHz Intel i7-6820EQ processor

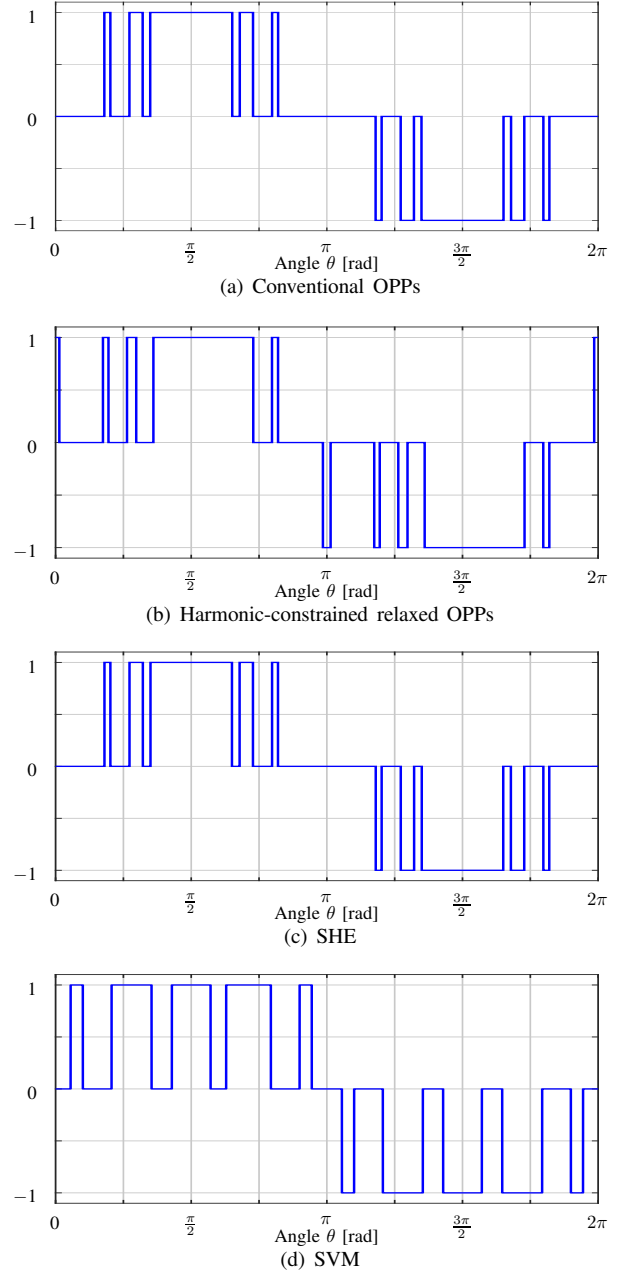


Fig. 6: Pulse patterns with $f_{sw} = 250$ Hz for $m = 0.79$ obtained from (a) the conventional OPP optimization problem, (b) the harmonic-constrained relaxed OPP optimization problem, (c) SHE, and (d) SVM.

and a Xilinx Kintex-7 filed-programmable gate array (FPGA) as the control platform. In addition, a PLECS RT-Box 1 simulates the power electronic system shown in Fig. 1 with a sampling interval of $T_{s,HIL} = 5 \mu s$. The RT-Box employs a Xilinx Zynq Z-7030 system-on-chip (SoC) as the processing unit, with its FPGA utilized to ensure high fidelity in real-time simulations through effective data acquisition (DAQ). This combination allows for precise and efficient handling of data, contributing to the accuracy and reliability of the overall system performance in the HIL setup. Moreover, the computed switching time instants t and corresponding switch positions u_{abc} are stored as look-up tables (LUTs) in the processor of the dSPACE and retrieved by its FPGA. Following, a counter-

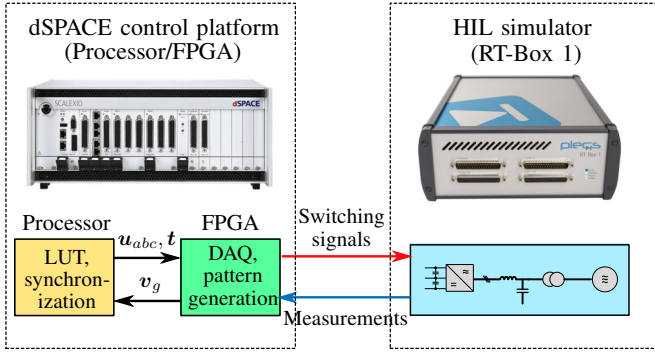


Fig. 7: Block diagram of the hardware-in-the-loop (HIL) test bench.

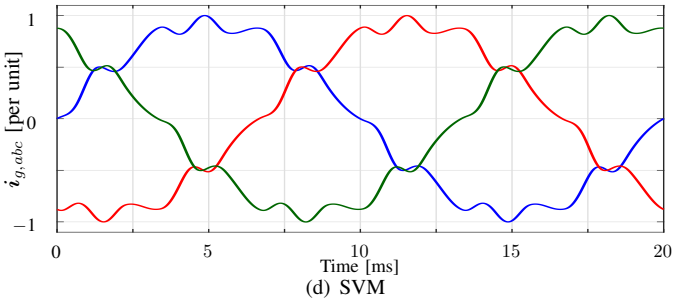
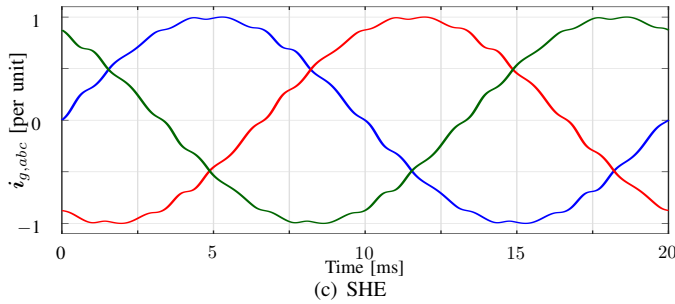
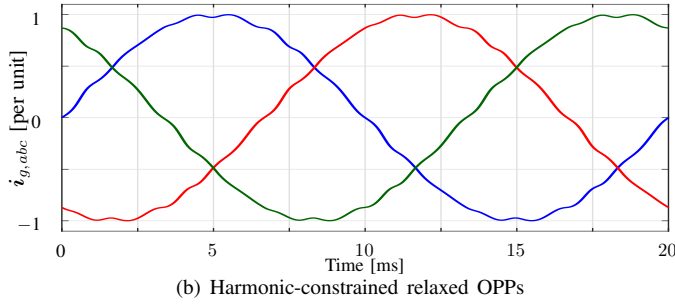
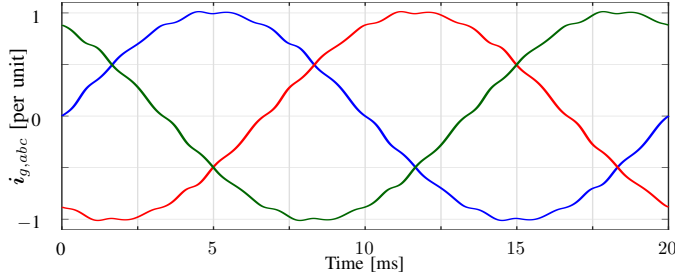
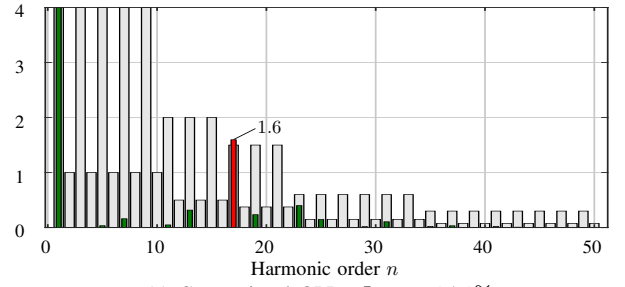
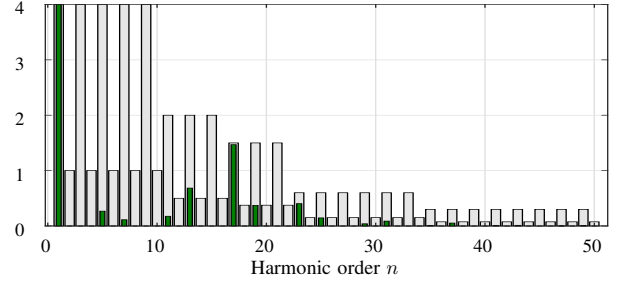


Fig. 8: Three-phase grid current produced by (a) the conventional OPPs, (b) the harmonic-constrained relaxed OPPs, (c) SHE, and (d) SVM, when operating at $m = 1.1185$.

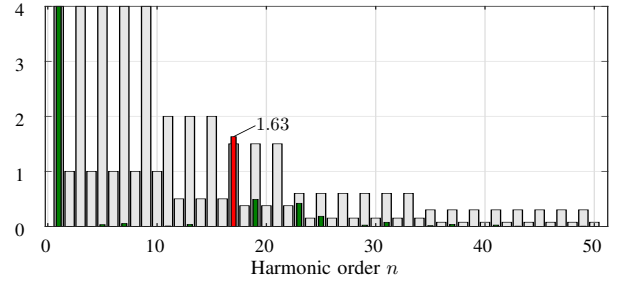
based mechanism within the FPGA regenerates the switching signals, which are transmitted to the RT-Box and applied to the power converter at the desired time instants.



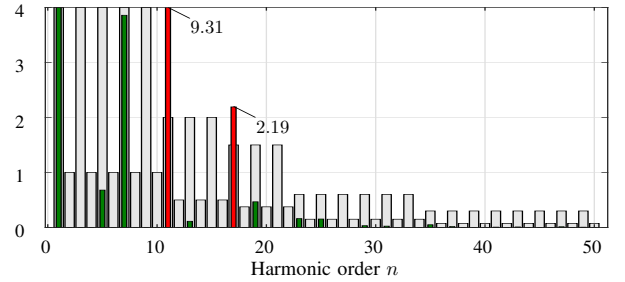
(a) Conventional OPPs; $I_{TDD} = 1.71\%$



(b) Harmonic-constrained relaxed OPPs; $I_{TDD} = 1.73\%$



(c) SHE; $I_{TDD} = 1.77\%$



(d) SVM; $I_{TDD} = 10.35\%$

Fig. 9: Grid current harmonics (%) for $m = 1.1185$. The limits dictated by the IEEE 519 standard are shown as light gray bars, current harmonics that meet them are shown as green bars, while harmonics that violate them are shown as red bars.

A. Nominal System Parameters

For the nominal system parameters provided in Tables I and II, and when operating at modulation index $m = 1.1185$ and switching frequency $f_{sw} = 250$ Hz, Fig. 8 illustrates the three-phase grid current over one fundamental period for the investigated PWM schemes. It is evident that, apart from SVM, all considered modulation techniques produce output currents with nearly identical levels of harmonic distortions. These findings are consistent with the numerical results presented in Fig. 4, confirming the accuracy of the real-time tests.

To provide more insight into the proposed OPPs, the grid current harmonic spectra for the discussed PWM techniques

at the selected operating point are presented in Fig. 9. Specifically, Fig. 9(a) illustrates the grid current harmonics produced by the conventional OPPs (i.e., those computed with (11)). Since these OPPs are computed by minimizing the current TDD, the resulting harmonic content is very low, achieving a TDD of just $I_{\text{TDD}} = 1.71\%$ despite the low switching frequency. However, there is no guarantee that individual current harmonics comply with harmonic grid standards, such as the considered IEEE 519 standard. This is evident in Fig. 9(a), where the 17th harmonic exceeds its permissible limit.

In contrast, the harmonic-constrained relaxed OPPs computed using (14) produce grid current harmonics that fully comply with the IEEE 519 standard, see Fig. 9(b). As indicated by the current TDD of 1.73%, the introduced harmonic limitations do not significantly compromise the overall current quality compared to the conventional OPPs. This favorable harmonic performance is due to the fact that the proposed OPPs are computed by relaxing QWS, providing more degrees of freedom in the optimization process to better manipulate the current harmonics.

Finally, the comparisons conclude with the current harmonic spectra resulting from the SHE and SVM techniques, see Figs. 9(c) and 9(d), respectively. Similar to the conventional OPPs, the computed SHE-based pulse patterns produce a grid current with the 17th harmonic exceeding the maximum allowable level. However, the achieved current TDD indicates that both OPPs and SHE yield similar levels of harmonic distortions for the considered operating point. In contrast, SVM leads to much higher harmonic content in the grid current and considerable violations for individual harmonics, see Fig. 9(d).

Based on the presented results, it can be concluded that the proposed OPPs outperform the modulation techniques against which they have been benchmarked. They not only produce very low values of current TDD—on par with conventional OPPs and SHE method—but also ensure that the generated harmonics fully comply with their permissible limits. This demonstrates the effectiveness of the proposed OPPs in achieving both high performance and adherence to harmonic grid standards.

B. Variations in Grid Impedance and Filter Components

Following, the robustness of the proposed OPPs to variations in the grid impedance and filter components is examined. In the first scenario, it is assumed that the grid impedance is 50% smaller than its nominal value (see Table II). The robustness of the examined PWM methods to such a variation is then investigated. As can be seen in Fig. 10, both the conventional OPPs and SHE-based pulse patterns result in the 17th harmonic exceeding the maximum allowable level. As for SVM, the harmonic content of the grid current is significant. In contrast, the proposed harmonic-constrained relaxed OPPs fully meet the IEEE 519 standard even with variations in the grid impedance, see Fig. 10(b). This is achieved by considering tighter upper limits $\hat{i}_{n,\max}$ in (14e). Nevertheless, it is worth noting that, while the cost of making the proposed OPPs robust

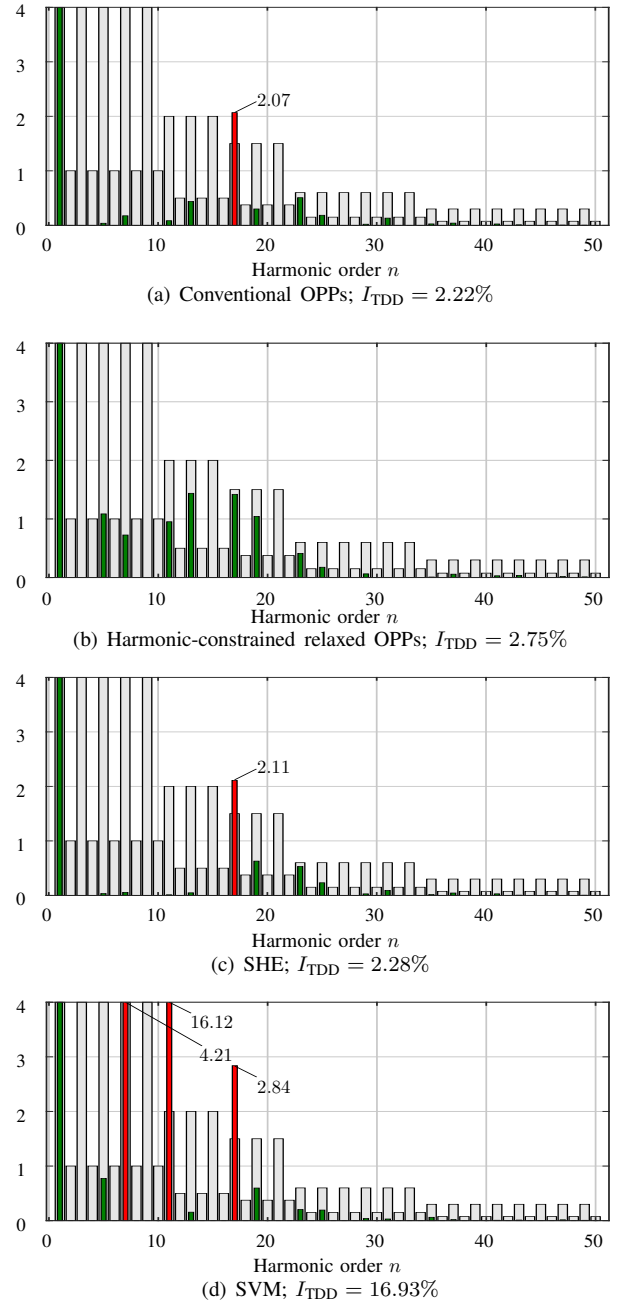
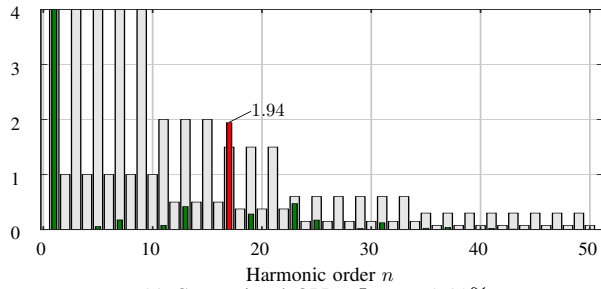


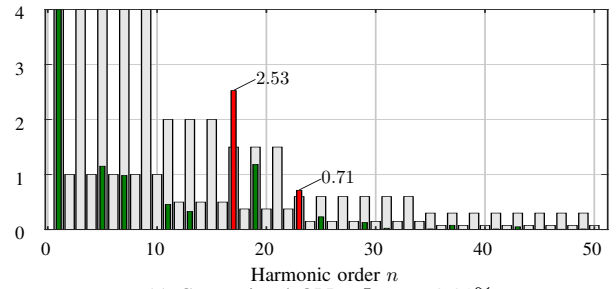
Fig. 10: Grid current harmonics (%) for $m = 1.1185$, while having variations in the grid impedance. The limits dictated by the IEEE 519 standard are shown as light gray bars, current harmonics that meet them are shown as green bars, while harmonics that violate them are shown as red bars.

is an increase in the current TDD, it remains well below the 5% limit required by the considered grid standard.

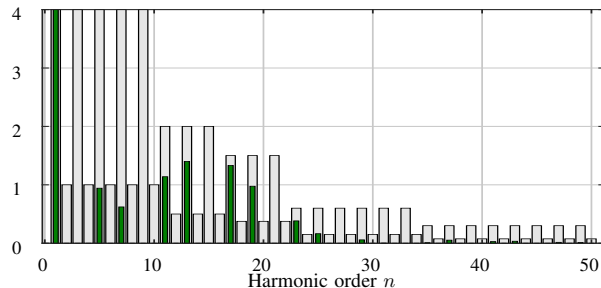
In the second scenario, it is assumed that the grid impedance is 10% smaller than its nominal value, while the filter inductance L_f and capacitance C experience a 5% degradation. The harmonic performance of grid current for the benchmarked PWM schemes is depicted in Fig. 11. A comparison of the harmonic spectra reveals that only the proposed harmonic-constrained relaxed OPPs are robust, maintaining compliance with grid standards despite variations in both filter components and grid impedance. Finally, it is important to note that although the current TDD of the proposed OPPs is higher



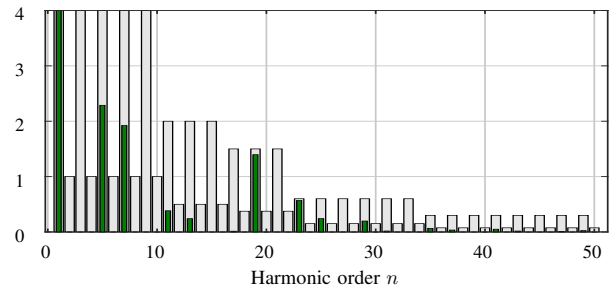
(a) Conventional OPPs; $I_{TDD} = 2.08\%$



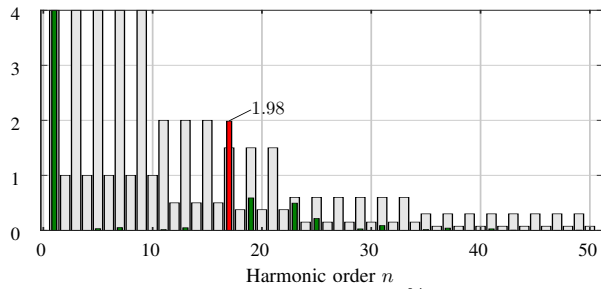
(a) Conventional OPPs; $I_{TDD} = 3.31\%$



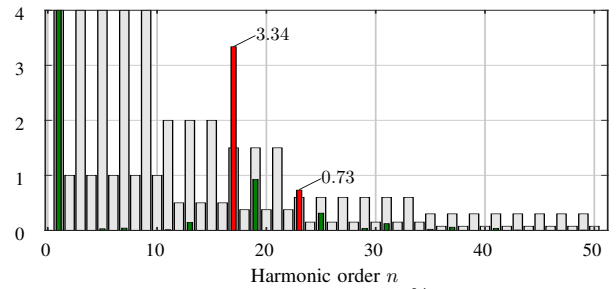
(b) Harmonic-constrained relaxed OPPs; $I_{TDD} = 2.65\%$



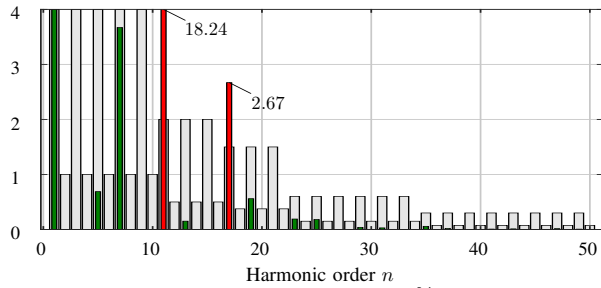
(b) Harmonic-constrained relaxed OPPs; $I_{TDD} = 3.33\%$



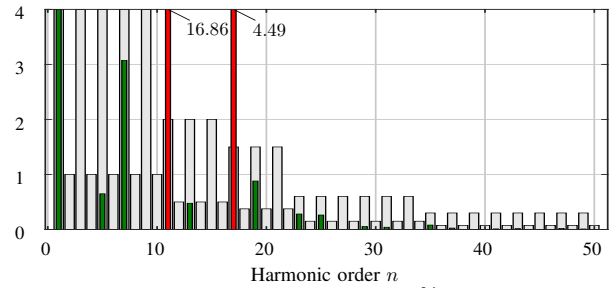
(c) SHE; $I_{TDD} = 2.14\%$



(c) SHE; $I_{TDD} = 3.56\%$



(d) SVM; $I_{TDD} = 18.82\%$



(d) SVM; $I_{TDD} = 17.76\%$

Fig. 11: Grid current harmonics (%) for $m = 1.1185$, while having variations in both filter components and grid impedance. The limits dictated by the IEEE 519 standard are shown as light gray bars, current harmonics that meet them as green bars, while harmonics that violate them are shown as red bars.

Fig. 12: Grid current harmonics (%) for $m = 1.1185$ and a smaller harmonic filter. The limits dictated by the IEEE 519 standard are shown as light gray bars, current harmonics that meet them as green bars, while harmonics that violate them are shown as red bars.

than that of the conventional OPPs and SHE, it remains well within the permissible range.

C. Reduced Harmonic Filter

To investigate the suitability of the examined PWM techniques with a smaller LCL filter, the inductance L_f and capacitance C of the nominal filter are reduced by 20%. Both conventional and proposed OPP optimization problems are solved considering the reduced filter parameters. This is in contrast to the SHE and SVM-based pulse patterns, which are independent of the filter characteristics. The resulting current harmonic spectra in Fig. 12 reveal that only the proposed OPPs

enable filter reduction while still abiding by the harmonic grid standards.

In stark contrast, the other examined modulation techniques result in individual current harmonics that exceed the limits imposed by the IEEE 519 standard. For instance, comparing the amplitude of the 17th current harmonic for the conventional OPPs and SHE-based pulse patterns (Figs. 12(a) and 12(c), respectively), the SHE method produces a significantly higher 17th harmonic. This is due to the fact that OPPs are computed to minimize the harmonic distortions. More impressively, the proposed harmonic-constrained relaxed OPPs can achieve a current TDD that is not only lower than that of SVM and

SHE, but also nearly identical to that of the conventional OPPs without harmonic constraints.

In addition, it should be pointed out that limiting the amplitude of a specific current harmonic often redistributes the harmonic content to other frequencies, see e.g., the 19th harmonic in Fig. 12(b). This could potentially result in standard violation for other harmonics. To address this issue, all nonzero low-frequency current harmonics are constrained in the OPP optimization problem (14), instead of merely imposing constraints on the harmonics that violate their limits.

In conclusion, the presented results clearly demonstrate the superior harmonic performance of the proposed OPPs, along with additional benefits such as filter size reduction. This can lead to lower hardware requirements and reduced system costs.

V. DISCUSSION

As shown in Sections III and IV, the proposed harmonic-constrained OPPs exhibit superior harmonic performance in ensuring compliance with harmonic grid standards, which is crucial for grid-connected converters. While these OPPs are equipped with robustness against system parameter variations, as demonstrated in Section IV-B, certain limitations remain. Specifically, since the offline optimization procedure is tailored to specific system parameters, it does not account for a wide range of parameter variations. Consequently, the harmonic performance may deteriorate under significantly different system parameters than those considered in the offline optimization or in the presence of persistent disturbances, such as prominent harmonics at the PCC injected by other sources [23].

To tackle this problem, one possible approach is to explicitly incorporate robustness into the optimization process, akin to [24]. For example, enhancing robustness against PCC disturbances and/or significant changes in system parameters—particularly the grid impedance—constitutes a relevant future research direction. However, it is worth noting that robustness often comes at the cost of more conservative solutions, meaning that OPPs designed for worst-case scenarios may compromise the current TDD in less challenging operating conditions.

To mitigate this trade-off and ensure optimal performance across all operating conditions, one alternative is to compute multiple OPPs for different scenarios. While this approach requires significantly higher computational effort, the offline nature of the optimization process makes this less critical. However, the memory required to store extensive LUTs that will contain the offline-computed OPPs could become a bottleneck, potentially limiting the real-time applicability of such an approach. In cases where memory constraints are an issue, learning-based algorithms—such as artificial neural networks—could provide a possible alternative for real-time OPP adaptation [17].

VI. CONCLUSIONS

This paper presented a new three-level OPP problem formulation for grid-connected converters with *LCL* filters. In addition to considering the filter transfer function from the switching signal to the output current, the OPP optimization problem

was augmented with explicit soft constraints on individual grid current harmonics. By doing so, the harmonic requirements—as dictated by relevant harmonic grid standards—are ensured while maintaining the best possible current quality. However, the introduction of harmonic constraints reduces the degrees of freedom in the current TDD minimization. To address the expected increase in current TDD, the traditional restrictions imposed on multilevel switching signals were relaxed, i.e., the quarter-wave symmetry was dropped and multipolar switch positions were allowed. This approach not only mitigated the increase in current TDD but also improved current quality within certain modulation intervals. As numerical results and real-time tests in a HIL environment verify, the proposed harmonic-constrained relaxed OPPs outperform SVM, SHE, and conventional OPPs in terms of compliance with grid standards. Moreover, the suggested formulation for the OPP problem enables effective shaping of the current harmonic spectrum, even when accounting for variations in filter components, grid impedance, and the use of a smaller filter. Hence, the proposed OPPs offer multidimensional benefits as not only they can fully respect harmonic grid standards while producing very low grid current TDD, but they also exhibit robustness against system parameter variations, and reduce filter requirements.

ACKNOWLEDGMENT

The authors would like to acknowledge the help of Isavella Koukoula with the HIL tests.

REFERENCES

- [1] D. G. Holmes and T. A. Lipo, *Pulse width modulation for power converters: Principles and practice*. Piscataway, NJ, USA: IEEE Press, 2003.
- [2] H. S. Patel and R. G. Hoft, "Generalized techniques of harmonic elimination and voltage control in thyristor inverters: Part I—Harmonic elimination," *IEEE Trans. Ind. Appl.*, vol. IA-9, no. 3, pp. 310–317, May/Jun. 1973.
- [3] W. Fei, X. Du, and B. Wu, "A generalized half-wave symmetry SHE-PWM formulation for multilevel voltage inverters," *IEEE Trans. Ind. Electron.*, vol. 57, no. 9, pp. 3030–3038, Sep. 2010.
- [4] M. S. A. Dahidah, G. Konstantinou, and V. G. Agelidis, "A review of multilevel selective harmonic elimination pwm: Formulations, solving algorithms, implementation and applications," *IEEE Trans. Power Electron.*, vol. 30, no. 8, pp. 4091–4106, Aug. 2015.
- [5] J. Nápoles, J. I. Leon, R. Portillo, L. G. Franquelo, and M. A. Aguirre, "Selective harmonic mitigation technique for high-power converters," *IEEE Trans. Ind. Electron.*, vol. 57, no. 7, pp. 2315–2323, Jul. 2010.
- [6] G. S. Buja and G. B. Indri, "Optimal pulsewidth modulation for feeding ac motors," *IEEE Trans. Ind. Appl.*, vol. IA-13, no. 1, pp. 38–44, Jan./Feb. 1977.
- [7] G. S. Buja, "Optimum output waveforms in PWM inverters," *IEEE Trans. Ind. Appl.*, vol. IA-16, no. 6, pp. 830–836, Nov./Dec. 1980.
- [8] R. Fotouhi, L. Leitner, R. Kennel, and H. du Toit Mouton, "An efficient method to calculate optimal pulse patterns for medium voltage converters," in *Proc. IEEE Ind. Electron. Conf.*, Dallas, TX, USA, Oct./Nov. 2014, pp. 1221–1226.
- [9] A. Birda, J. Reuss, and C. M. Hackl, "Synchronous optimal pulsewidth modulation for synchronous machines with highly operating point dependent magnetic anisotropy," *IEEE Trans. Ind. Electron.*, vol. 68, no. 5, pp. 3760–3769, May 2021.
- [10] J. A. Pontt, J. R. Rodriguez, A. Liendo, P. Newman, J. Holtz, and J. M. S. Martin, "Network-friendly low-switching-frequency multipulse high-power three-level pwm rectifier," *IEEE Trans. Ind. Electron.*, vol. 56, no. 4, pp. 1254–1262, Apr. 2009.

- [11] A. K. Rathore, J. Holtz, and T. Boller, "Synchronous optimal pulsewidth modulation for low-switching-frequency control of medium-voltage multilevel inverters," *IEEE Trans. Ind. Electron.*, vol. 57, no. 7, pp. 2374–2381, Jul. 2010.
- [12] IEEE Std 519-2014 (Revision of IEEE Std 519-1992), "IEEE recommended practices and requirements for harmonic control in electrical power systems," pp. 1–29, Jun. 2014.
- [13] J. Pontt, J. Rodriguez, and R. Huerta, "Mitigation of noneliminated harmonics of SHEPWM three-level multipulse three-phase active front end converters with low switching frequency for meeting standard IEEE-519-92," *IEEE Trans. Power Electron.*, vol. 19, no. 6, pp. 1594–1600, Nov. 2004.
- [14] A. Moeini, H. Iman-Eini, and M. Bakhshizadeh, "Selective harmonic mitigation—pulse-width modulation technique with variable dc-link voltages in single and three-phase cascaded H-bridge inverters," *IET Power Electron.*, vol. 7, no. 4, pp. 924–932, Apr. 2014.
- [15] M. Najjar, A. Moeini, M. K. Bakhshizadeh, F. Blaabjerg, and S. Farhangi, "Optimal selective harmonic mitigation technique on variable dc link cascaded H-bridge converter to meet power quality standards," *IEEE J. Emerg. Sel. Topics Power Electron.*, vol. 4, no. 3, pp. 1107–1116, Sept. 2016.
- [16] A. Moeini, H. Zhao, and S. Wang, "A current-reference-based selective harmonic current mitigation PWM technique to improve the performance of cascaded H-bridge multilevel active rectifiers," *IEEE Trans. Ind. Electron.*, vol. 65, no. 1, pp. 727–737, Jan. 2018.
- [17] I. Ibanez-Hidalgo, A. Sanchez-Ruiz, A. Perez-Basante, A. Zubizarreta, S. Ceballos, S. Gil-Lopez, and R. P. Aguilera, "Real time selective harmonic control—PWM based on artificial neural networks," *IEEE Trans. Power Electron.*, vol. 39, no. 1, pp. 768–783, Jan. 2024.
- [18] L. G. Franquelo, J. Nápoles, R. C. P. Guisado, J. I. León, and M. A. Aguirre, "A flexible selective harmonic mitigation technique to meet grid codes in three-level PWM converters," *IEEE Trans. Ind. Electron.*, vol. 54, no. 6, pp. 3022–3029, Dec. 2007.
- [19] J. Nápoles, A. J. Watson, J. J. Padilla, J. I. León, L. G. Franquelo, P. W. Wheeler, and M. A. Aguirre, "Selective harmonic mitigation technique for cascaded H-bridge converters with nonequal dc link voltages," *IEEE Trans. Ind. Electron.*, vol. 60, no. 5, pp. 1963–1971, May 2013.
- [20] T. Dorfling, H. d. T. Mouton, and T. Geyer, "Generalized model predictive pulse pattern control based on small-signal modeling—Part 2: Implementation and analysis," *IEEE Trans. Power Electron.*, vol. 37, no. 9, pp. 10 488–10 498, Sep. 2022.
- [21] S. Rahmanpour, P. Karamanakos, and T. Geyer, "Three-level optimized pulse patterns for grid-connected converters with *LCL* filters," in *Proc. IEEE Energy Convers. Congr. Expo.*, Nashville, TN, USA, Oct. 2023, pp. 1430–1437.
- [22] A. Birth, T. Geyer, H. d. T. Mouton, and M. Dorfling, "Generalized three-level optimal pulse patterns with lower harmonic distortion," *IEEE Trans. Power Electron.*, vol. 35, no. 6, pp. 5741–5752, Jun. 2020.
- [23] S. Rahmanpour, P. Karamanakos, and T. Geyer, "Optimized pulse patterns for converters connected to a distorted grid via *LCL* filters," in *Proc. IEEE Energy Convers. Congr. Expo. Eur.*, Darmstadt, Germany, Sep. 2024, pp. 1–8.
- [24] O. Karaca and I. Tsoumas, "Robust optimized pulse patterns for salient permanent magnet synchronous machines," in *Proc. Eur. Conf. on Power Electron. and Applicat.*, Aalborg, Denmark, Sep. 2023, pp. P.1–P.9.



Shirin Rahmanpour (S'23) received the B.S. and M.S. degrees in electrical engineering-control from the Sahand University of Technology, Tabriz, Iran, in 2014, and 2018, respectively.

Since 2022, she has been with the Faculty of Information Technology and Communication Sciences, Tampere University, Tampere, Finland, where she is currently working toward the Ph.D. degree in computing and electrical engineering. Her main research interests include optimal modulation, mathematical programming, and power electronics.



Petros Karamanakos (M'14 – SM'19) received the Diploma and Ph.D. degrees in electrical and computer engineering from the National Technical University of Athens (NTUA), Athens, Greece, in 2007, and 2013, respectively.

From 2010 to 2011 he was with the ABB Corporate Research Center, Baden-Dättwil, Switzerland, where he worked on model predictive control strategies for medium-voltage drives. From 2013 to 2016 he was a PostDoc Research Associate in the Chair of Electrical Drive Systems and Power Electronics, Technische Universität München, Munich, Germany. Since 2016, he has been with the Faculty of Information Technology and Communication Sciences, Tampere University, Tampere, Finland, where he is currently an Associate Professor. His main research interests lie at the intersection of optimal control, mathematical programming, and power electronics, including model predictive control and optimal modulation for utility-scale power converters and ac variable speed drives.

Dr. Karamanakos has received three IEEE journal paper awards and five prize paper awards at IEEE conferences. He serves as an Associate Editor of the IEEE Transactions on Power Electronics, IEEE Journal of Emerging and Selected Topics in Power Electronics, and IEEE Transactions on Industry Applications. He has been a Regional Distinguished Lecturer of the IEEE Power Electronics Society since 2022.



Tobias Geyer (M'08 – SM'10 – F'22) received the Dipl.-Ing. degree in electrical engineering, the Ph.D. degree in control engineering, and the Habilitation degree in power electronics from ETH Zurich, Zurich, Switzerland, in the years 2000, 2005 and 2017, respectively.

After his Ph.D., he spent three years at GE Global Research, Munich, Germany, three years at the University of Auckland, Auckland, New Zealand, and eight years at ABB's Corporate Research Centre, Baden-Dättwil, Switzerland. In 2020, he joined ABB's Medium-Voltage Drive division as R&D Platform Manager of the ACS6000 and ACS6080. In 2022, he became a Corporate Executive Engineer. He has been an extraordinary Professor at Stellenbosch University, Stellenbosch, South Africa, since 2017.

He is the author of more than 40 patent families, 170 publications, and the book "Model predictive control of high power converters and industrial drives" (Wiley, 2016). He teaches a regular course on model predictive control at ETH Zurich. His research interests include medium-voltage and low-voltage drives, utility-scale power converters, optimized pulse patterns and model predictive control.

Dr. Geyer received the IEEE PELS Modeling and Control Technical Achievement Award in 2022, the Semikron Innovation Award in 2021, and the Nagamori Award in 2021. He also received two Prize Paper Awards of IEEE Transactions and three Prize Paper Awards at IEEE conferences. He is a former Associate Editor of the IEEE Transactions on Industry Applications (from 2011 until 2014) and the IEEE Transactions on Power Electronics (from 2013 until 2019). He was an International Program Committee Vice Chair of the IFAC conference on Nonlinear Model Predictive Control in Madison, WI, USA, in 2018. Dr. Geyer was a Distinguished Lecturer of the IEEE Power Electronics Society from 2020 to 2023.